Chapter 18
Density-Graded 3D Voronoi Cellular Structures for Improved Impact Performance

Vijendra Gupta, Addis Kidane, and Michael Sutton

Abstract Density-graded cellular polymers have unique mechanical properties, leading to exceptional impact protection. Furthermore, they can be designed for custom requirements. The current study is part of an effort to develop efficient impact-resistant structures. The impact response of density-graded 3D Voronoi cellular structures is studied and compared to its uniform density counterpart. The specimens are fabricated via photopolymer jetting technology, an additive manufacturing technique that enables high accuracy of intricate features and complex shapes that are distinctive of Voronoi cellular structures. The density gradation is achieved by changing the cell size along the impact direction. The foam specimens are impinged by a freely falling rigid mass with the help of a drop tower that allows determining the response at intermediate strain-rate regime. A series of images are captured using a high-speed camera to capture the deformation mechanisms of the specimen, and a piezo-based load cell is used to measure the dynamic force. The performance is analyzed by studying the energy absorption and transmitted force as a function of density gradation. It is found that density-graded Voronoi cellular structures can be designed to mitigate a wide range of impact conditions.

Keywords 3D printing · Voronoi cellular structures · Density-graded cellular materials · Impact response · Energy absorption

18.1 Introduction

Cellular structures with remarkable engineering properties are commonly found in nature [1]. Exceptional performance can be derived if the key design elements of natural cellular structures are purposefully harnessed. In particular, the density gradation observed in the natural environment can be utilized in engineering structures to obtain superior functionality. As a result, density-graded Voronoi cellular structures (VCSs) that have structural similarities to naturally existing cellular structures have gained tremendous attention. These structures have excellent energy absorption capacity and provide protection from a broad range of impact situations.

There have been numerous studies on VCSs. Theoretical studies [2–5] often model the cellular material as a continuum to simplify and obtain a solution, whereas finite element studies employ either continuum-based [4, 6] or cell-based approaches [3, 7, 8]. Although the cell-based models are complex due to the manifestation of microstructural details, they provide a deep understanding of the deformation mechanisms. Experimental investigations often are performed on layered specimens that comprise a step-wise change in density [8, 9]. In addition to their tedious fabrication, layered specimens have interfaces that are prone to debonding. Cellular materials with gradually varying density eliminate the aforementioned issues. However, manufacturing such structures has been a challenge due to the geometrical complexities associated with compliance to a specified spatial density variation. This impediment can be efficiently tackled by employing additive manufacturing such as photopolymer jetting technology employed in the current study. This 3D printing technique readily addresses the fabrication of complicated parts with elaborate features and enables the production of specimens with continuous changes in properties.

This study investigates the dynamic response of additively manufactured 3D VCSs under low-impact velocities. Uniform density and density-graded specimens are prepared by controlling the local cell size. The specimens are subjected to rigid body impact with the help of a drop tower setup, and their energy absorption performance is analyzed.

V. Gupta (✉) · A. Kidane · M. Sutton
Department of Mechanical Engineering, University of South Carolina, Columbia, SC, USA
e-mail: vijendra@email.sc.edu; kidanea@cec.sc.edu; sutton@sc.edu

18.2   Materials and Methods

Voronoi cells are the building blocks of VCSs. They are convex polyhedrons constructed around randomly generated points that form their cell nuclei. Each Voronoi cell has its corresponding cell nucleus. The nucleus of a particular Voronoi cell is the nearest one to all the points within that cell. The edges of the cell are the common boundaries between the adjacent cells, formed by points that are equidistant to the nearest cell nuclei. Random generation of cell nuclei is performed with a constraint such that every cell nucleus is at least a specified distance (d_{min}) away from all other cell nuclei. Thus, the local density can be influenced by the distance d_{min}. Uniform density specimens are constructed with a constant d_{min}, while the density-graded specimens are prepared by varying d_{min}. The VCS model results in large geometrical data that is processed by Python scripting. The solid model is then created and rendered in stereolithography (STL) file format using OpenSCAD, an open-sourced application program. Afterward, printing is carried out on a multi-jet 3D printer, namely, the Stratasys J750. The printer is based on a principle that takes advantage of the sensitivity of certain polymers to light. It prints a photosensitive polymer layer-by-layer that is instantly cured by ultraviolet light. The printed part is cleaned in an alkaline solution before it is completely prepared.

Both the uniform density and density-graded specimens are printed in cylindrical form with a radius of 16 mm and a height of 35 mm. The specimen photographs are shown in Fig. 18.1a. Cell size is roughly kept the same in the uniform specimens, while it is reduced gradually from top to bottom in the graded specimens (as seen in the figure). The specimens are designed such that their average densities are very close for an appropriate comparison. The average density of the uniform specimen and the graded specimen is measured to be 62.8 kg/m^3 and 64.4 kg/m^3, respectively.

The compressive dynamic response of the 3D-printed specimens is assessed by impacting them with a freely falling rigid mass made of stainless steel. Figure 18.1b shows the schematic of the experimental setup. The rigid mass is guided through a hollow tube mounted on the drop tower frame. The drop height is 9.15 cm, and the rigid mass weighs 0.857 kg. A piezoelectric-based impact load sensor is mounted below the specimen to measure the dynamic force in the specimen. To evenly transfer the load, a 5 mm thick rigid plate is placed in between the specimen and the force sensor. The load data is acquired at 0.25 MHz with the help of an amplifier and an oscilloscope. The strain in the specimen is determined by tracking the rigid mass using digital image correlation (DIC). A contrasting pattern is applied to the falling rigid mass, and its image sequence is captured using a high-speed camera to measure the displacement history. The images are recorded at an interframe time of 0.2 ms.
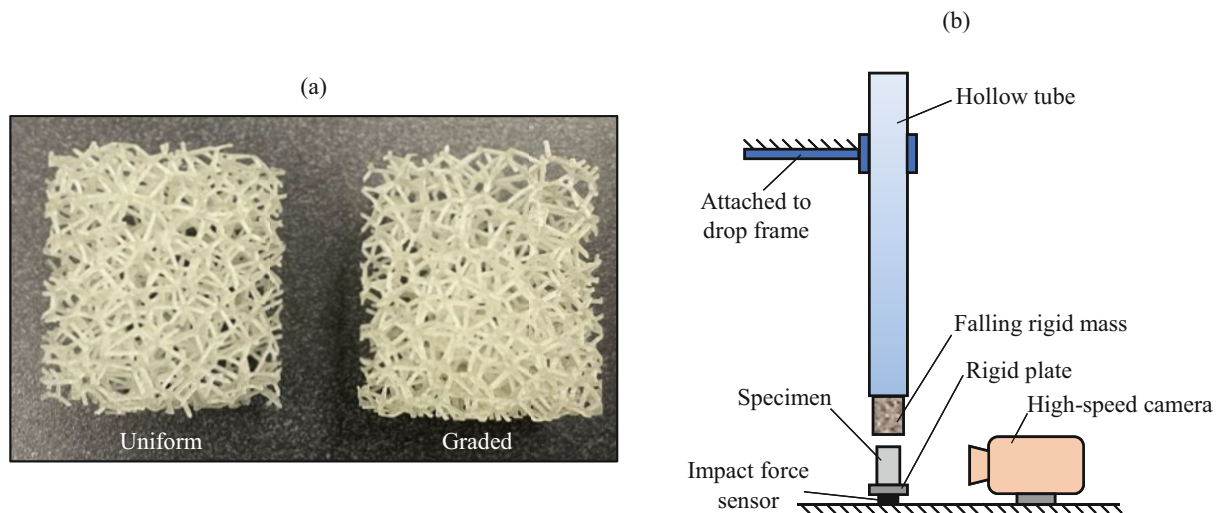

Fig. 18.1 (**a**) Specimen photographs. (**b**) Schematic of the experimental setup

18.3 Results and Discussion

The recorded load data is shown in Fig. 18.2. The noise present in the raw data is removed using the Savitzky-Golay filter [10]. A second-order polynomial and a window size of 201 points, equivalent to 0.8 ms on the time scale, are used for smoothing the data. These settings give adequately smoothed data without losing key features. The raw and smoothed data for the uniform specimen are shown in Fig. 18.2a for reference. The time data is shifted such that the rigid mass strikes the specimen at time $t = 0$. Figure 18.2b shows the force data for both the uniform and the graded specimen. It should be noted that the same smoothing parameters are used for the data of both specimens.

The rigid mass displacement obtained from DIC is depicted in Fig. 18.3. It increases almost linearly with time for both specimens, with the slope of the curves gradually reducing over time as the kinetic energy of the rigid mass is dissipated.

The force and displacement data are normalized using the continuum basis. The nominal stress σ is defined as the force per unit cross-sectional area, whereas the nominal strain ε is defined as the change in length per unit original length. It should be noted that the rigid mass displacement is equal to the change in specimen length. The nominal stress-strain curve is shown in
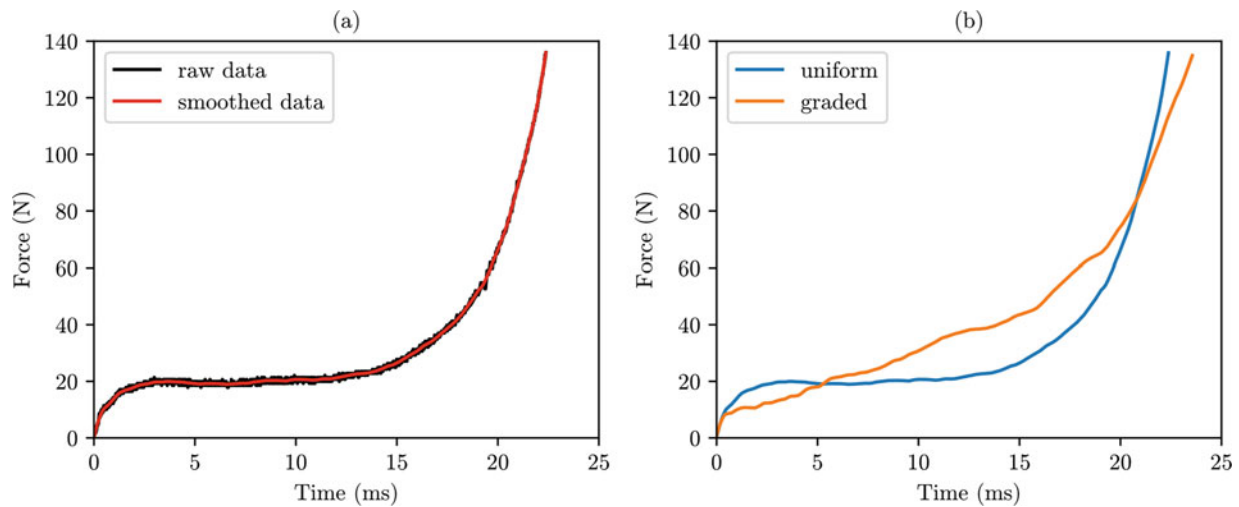
Fig. 18.2 (**a**) Raw and filtered (smoothed) force data for the uniform specimen (**b**) Force data for both the uniform and graded specimen
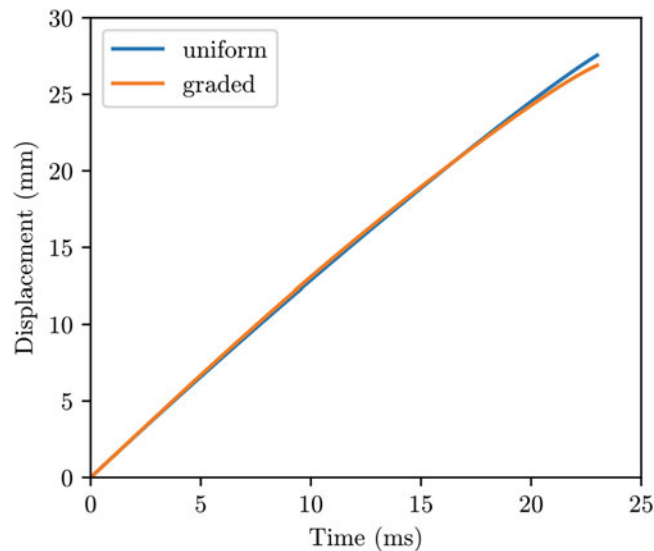
Fig. 18.3 Displacement histories for both the uniform and graded specimen
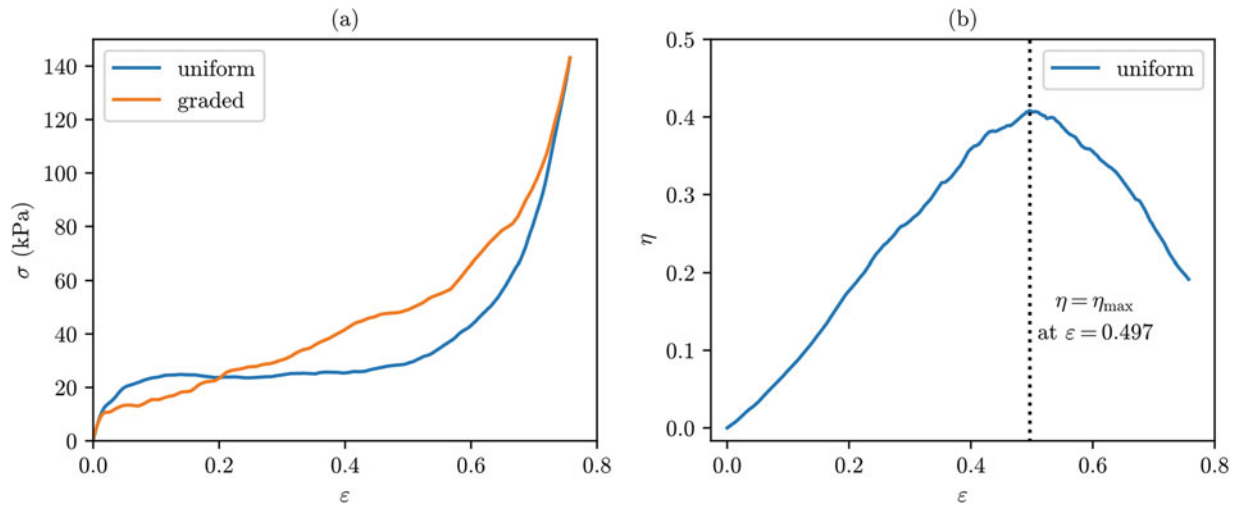
Fig. 18.4 (**a**) Stress-strain curves (**b**) Efficiency-strain curve for the uniform specimen

Fig. 18.4a. The main difference between the response of uniform and graded specimen is seen in the plateau region. If minor aberrations are ignored, the uniform specimen has a flat plateau. In other words, the stress remains approximately constant stress in the plateau region for the uniform specimen. On the other hand, the graded specimen has a plateau with a positive slope, or the stress steadily increases in the plateau region for the graded specimen. The difference in the behavior is due to the disparity in the cell sizes that make up the specimens. Since the uniform specimen is comprised of similar-sized cells, it crushes at approximately the same stress. However, the graded specimen consists of cells that vary in size. Therefore, the cells successively collapse based on their strength. The larger cells that are weaker collapse at low stress, while the smaller cells collapse at higher stress, thus resulting in a plateau characterized by an increasing slope.

The energy absorbed by the specimen E can be determined by computing the area under the stress-strain curve, and is given by the following equation:

$$E = \int_0^\varepsilon \sigma \mathrm{d}\varepsilon \tag{18.1}$$

The energy absorption efficiency η defined as the ratio of the energy absorbed and the stress is given as follows.

$$\eta = \frac{E}{\sigma} \tag{18.2}$$

Figure 18.4b shows the plot for the efficiency of the uniform specimen. The densification strain ε_d can be determined using the maximum efficiency method [11]. According to this method, densification of the specimen occurs when the efficiency reaches its maximum. Therefore, the densification strain is found to be 49.7% for the uniform specimen. The plateau stress σ_pl is calculated by Eq. (18.3) once the densification strain is known.

$$\sigma_\mathrm{pl} = \frac{1}{\varepsilon_\mathrm{d} - \varepsilon_\mathrm{cr}} \int_{\varepsilon_\mathrm{cr}}^{\varepsilon_\mathrm{d}} \sigma \mathrm{d}\varepsilon \tag{18.3}$$

where ε_cr is the strain at the initial collapse stress. Since ε_cr is very small, it can be ignored for the calculation of plateau stress. Using numerical integration, the plateau stress is computed to be 23.7 kPa.

Figure 18.5a shows the graph with stress as the abscissa and absorbed energy as the ordinate. A reference line corresponding to the plateau stress of the uniform specimen is also shown in the figure. Below the plateau stress of the uniform specimen, the graded specimen absorbs a higher amount of energy than the uniform specimen. However, around the plateau stress, the energy absorption of the uniform specimen increases dramatically, exceeding that of the graded specimen.
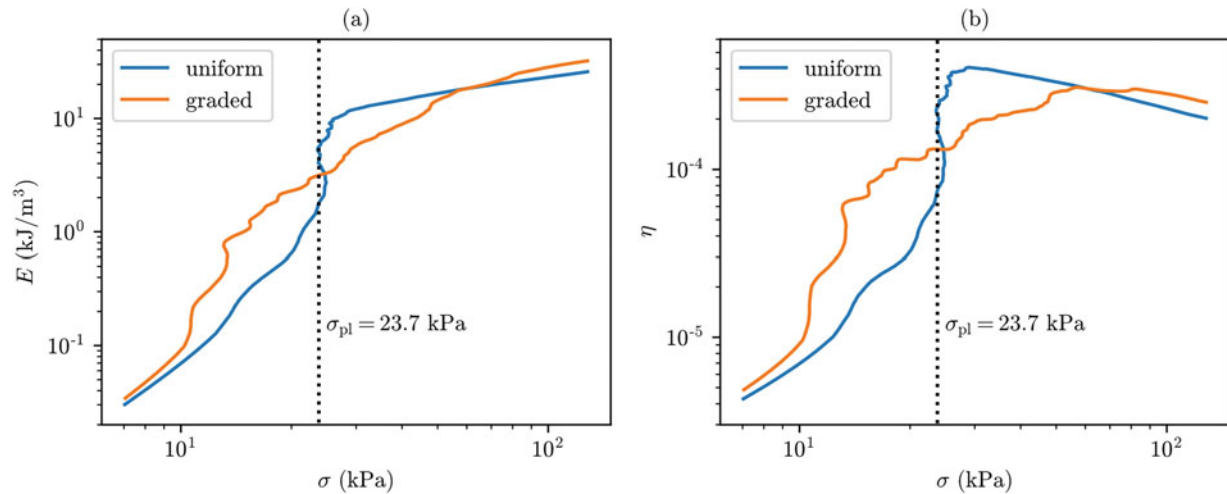
Fig. 18.5 (**a**) Energy versus stress plot (**b**) Efficiency versus stress plot

At high stress, the graded specimen again surpasses the uniform specimen since the latter can maintain higher energy absorption only up to a certain stress level. For most of the stress spectrum, the graded specimen remains superior. The uniform specimen performs better only in the moderate stress range. Therefore, the graded specimen has better performance for a wide range of energy levels. The plot of efficiency versus stress that shows similar trends is also shown in Fig. 18.5b. A uniform density can be designed to meet an energy requirement that is known with high certainty. However, its performance is poor if there is any variation in the energy input. In practice, the requirements are often known with high uncertainty. Graded specimens remain efficient over a wide range of energy levels, thereby making them more robust and versatile.

18.4 Conclusions

Voronoi cellular structures with complicated features are additively manufactured using photopolymer jetting technology, which otherwise is challenging to fabricate using conventional manufacturing approaches. Their energy absorption performance is evaluated using a drop tower setup. It has been shown that the dynamic responses of the uniform-density and density-graded Voronoi cellular specimens are significantly different. The uniform specimen possesses a flat plateau in its stress-strain curve, whereas the graded specimen has a characteristic increasing slope in the plateau region. These distinctive features result in differing energy absorption capabilities. Although the energy absorption of the uniform specimen is optimized for moderate energy input, its performance deteriorates at low and high energy input levels. On the other hand, the graded specimen outperforms at low and high energy inputs, and its performance does not significantly deteriorate at moderate energy inputs. Thus, density-graded Voronoi cellular structures provide all-round energy absorption performance.

References

1. Gibson, L.J., Ashby, M.F.: Cellular Solids, Second. Cambridge University Press (1997)
2. Gupta, V., Kidane, A., Sutton, M.: Closed-form solution for shock wave propagation in density-graded cellular material under impact. Theor. Appl. Mech. Lett. **11**(5), 100288 (2021). https://doi.org/10.1016/j.taml.2021.100288
3. Wang, X., Zheng, Z., Yu, J.: Crashworthiness design of density-graded cellular metals. Theor. Appl. Mech. Lett. **3**(3), 031001 (2013). https://doi.org/10.1063/2.1303101
4. Shen, C.J., Lu, G., Yu, T.X.: Investigation into the behavior of a graded cellular rod under impact. Int. J. Impact Eng. **74**, 92–106 (2014). https://doi.org/10.1016/j.ijimpeng.2014.02.015

5. Gupta, V., Miller, D., Kidane, A., Sutton, M.: Optimization for Improved Energy Absorption and the Effect of Density Gradation in Cellular Materials, pp. 13–20 (2021). https://doi.org/10.1007/978-3-030-59765-8_4

6. Cui, L., Kiernan, S., Gilchrist, M.D.: Designing the energy absorption capacity of functionally graded foam materials. Mater. Sci. Eng. A. **507**(1–2), 215–225 (2009). https://doi.org/10.1016/j.msea.2008.12.011

7. Zhang, J., Wang, Z., Zhao, L.: Dynamic response of functionally graded cellular materials based on the Voronoi model. Compos. Part B Eng. **85**, 176–187 (2016). https://doi.org/10.1016/j.compositesb.2015.09.045

8. Gupta, V., Miller, D., Kidane, A.: Numerical and Experimental Investigation of Density Graded Foams Subjected to Impact Loading, pp. 31–35 (2020). https://doi.org/10.1007/978-3-030-30021-0_6

9. Miller, D., Gupta, V., Kidane, A.: Dynamic Response of Layered Functionally Graded Polyurethane Foam with Nonlinear Density Variation, pp. 25–30 (2020). https://doi.org/10.1007/978-3-030-30021-0_5

10. Savitzky, A., Golay, M.J.E.: Smoothing and Differentiation of Data by Simplified Least Squares Procedures. ICASSP, IEEE Int. Conf. Acoust. Speech Signal Process. – Proc. **36**(8), 1627–1639 (1964). https://doi.org/10.1109/ICASSP.2000.859059

11. Tan, P.J., Harrigan, J.J., Reid, S.R.: Inertia effects in uniaxial dynamic compression of a closed cell aluminium alloy foam. Mater. Sci. Technol. **18**(5), 480–488 (2002). https://doi.org/10.1179/026708302225002092